

Nature of the orbital angular momentum (OAM) fields in a multilayered fiber

RAMESH BHANDARI

Laboratory for Physical Sciences, 8050 Greenmead Drive, College Park, Maryland 20740, USA
rbhandari@lps.umd.edu

Abstract: We provide a theoretical analysis of the nature of the orbital angular momentum (OAM) modal fields in a multilayered fiber, such as the step-index fiber and the ring-core fiber. In a detailed study of the vector field solutions of the step-index fiber (in the exponential basis) we discover that the polarization-induced field component is a modified scalar OAM field (as opposed to a standard OAM scalar field) with a shifted intensity pattern in the weakly guiding approximation (WGA); the familiar intensity donut pattern is reduced or increased in radius depending upon whether it is a case of spin-alignment or anti-alignment with the OAM. Such a shift in the intensity pattern appears to be a general feature of the field of a multilayered fiber as seen from an extension to the ring-core fiber. Additionally, we derive a general expression for the polarization-correction to the scalar propagation constant, which includes, for the first time, the contribution of the polarization-induced field. All the analytic expressions are illustrated and validated numerically with application to a step-index fiber, whose analytic solutions are well-known.

© 2021 Optical Society of America under the terms of the [OSA Open Access Publishing Agreement](#)

1. Introduction

Because of the possibility of a multifold increase in data-carrying capacity on an optical fiber, research in orbital angular momentum propagation (OAM) mode propagation in a fiber has proliferated. The orthogonality of the OAM modes makes possible the augmentation of fiber capacity by stacking different streams of data on different OAM modes, characterized by a unique set of topological charge, radial index number, and polarization, but possessing the same wavelength. The topological charge, usually denoted l , is representative of the orbital angular momentum $l\hbar$ per photon carried by the mode.

The vector OAM modes are the solutions, $HE_{l+1,m}$ and $EH_{l-1,m}$, of the vector wave equation when solved directly in the $e^{\pm il\theta}$ basis [1], where θ is the azimuthal angle in the cylindrical polar coordinates (this is in sharp contrast to the $\cos l\theta, \sin l\theta$ basis, traditionally used within the optics community, which by and large treats wave propagation in terms of even and odd modes as in [2]; in this basis, the OAM solutions are subsequently constructed through linear combinations of the even $\cos(l\theta)$ and odd $\sin(l\theta)$ solutions; see, e.g., [3–5]). In what follows, we suppress the radial index m for convenience; however, all numerical calculations assume $m = 1$. The transverse fields of the vector OAM modes, HE_{l+1} and EH_{l-1} , denoted $\vec{e}_t^{(l+1)}$ and $\vec{e}_t^{(l-1)}$, respectively, satisfy the wave equation

$$(\nabla_t^2 + k^2 n^2(r))\vec{e}_t^{(l\pm 1)} + \vec{\nabla}_t(\vec{e}_t^{(l\pm 1)} \cdot \vec{\nabla}_t \ln(n^2)) = \beta_{l\pm 1}^2 \vec{e}_t^{(l\pm 1)}, \quad (1)$$

where the third term on the left-hand-side incorporates all the *polarization effects*; β_{l+1} and β_{l-1} are, respectively, the corresponding propagation constants that are determined from two different characteristic equations, one corresponding to the HE_{l+1} modes and the other to the EH_{l-1} modes [2]; $k = 2\pi/\lambda$, where λ is the wavelength. We assume here that refractive index n is given by the familiar expression: $n^2 = n_1^2(1 - 2\Delta f(r))$, where $n_1, n_2, f(r), \Delta (= (n_1^2 - n_2^2)/(2n_1^2))$ are respectively the refractive index of the core, the refractive index of the cladding, index profile

function, and the profile height parameter (as in the commercial step-index fiber or the currently investigated ring-core fiber [3, 6, 7]; see Fig. 1). Thus, when $n_2 \rightarrow n_1$, $\Delta \rightarrow 0$, rendering $\vec{\nabla}_t \ln(n^2) = 0$ in Eq. 1; in other words, the polarization effects disappear in the limit $n_2 \rightarrow n_1$, and Eq. 1 reduces to a scalar wave equation:

$$(\nabla_t^2 + k^2 n^2(r)) \vec{e}_t^{(l)} = \tilde{\beta}_l^2 \vec{e}_t^{(l)}, \quad (2)$$

where $\vec{e}_t^{(l)} = F_l(r) e^{il\theta} \vec{e}_\pm$ is a derivative of $\vec{e}_t^{(l\pm 1)}$ in the limit $n_2 \rightarrow n_1$ (see Appendix A), and $\tilde{\beta}_l$ is the corresponding scalar propagation constant (in this limit the two different characteristic equations for the vector modes reduce to a single characteristic equation for the scalar OAM mode with topological charge l and propagation constant $\tilde{\beta}_l$). For the general case, $\Delta < 1$, we can make an expansion of $\ln(n^2)$ in the parameter Δ . In the *weakly guiding approximation* (WGA), where $\Delta \ll 1$, expansion to first order in Δ suffices, which then yields $\vec{\nabla}_t \ln(n^2) = -2\Delta(\partial f(r)/\partial r)\hat{r}$ in Eq. 1. We therefore expect the polarization correction to the propagation constant

$$\delta\beta_{l\pm 1}^2 = \beta_{l\pm 1}^2 - \tilde{\beta}_l^2 \quad (3)$$

and the field correction

$$\delta\vec{e}_t^{(l\pm 1)} = \vec{e}_t^{(l\pm 1)} - \vec{e}_t^{(l)} \quad (4)$$

to be each of order Δ . We refer to this field correction as *polarization-induced* due to its dependence on the parameter Δ . Analytic expressions up to order Δ have been given for Eq. 3 in [2] (in the context of the scalar *LP* modes) and by [8–10] (in the context of scalar OAM modes); specifically in [10], explicit expressions for polarization correction to the scalar propagation constant to first order for the step-index fiber are given (note that the polarization corrections for the OAM modes and the corresponding *LP* modes are identical because they are the solutions of the same scalar wave equation, and the scalar OAM modal fields and the *LP* modes are linearly related). Regarding Eq. 4, a correction to order Δ in the context of *LP* modes has also been cited in [2], but no analytic expression is provided therein. The field correction can also be determined in perturbation theory [1, 11, 12], but the obtained expression is an approximation expressed in terms of the fields of the traditional scalar modes.

In this paper, we derive the exact analytic expressions for the vector fields in multilayered fibers such as the step-index fiber and the ring-core fiber (Fig. 1), and subject them to close scrutiny for their OAM contents. The structure of the polarization-induced OAM field is especially studied. Subsequently, we ascertain its impact on the polarization correction to the propagation constant of the scalar modes. We begin in Section 2 with the basic definitions and concepts, constructing in the process the general OAM composition of the vector fields of a circular fiber, along with the related concept of the total angular momentum, $J = L + S$. Subsequently (in Section 3), we derive an analytic form of the vector field solutions for the step-index fiber, which is then examined for its OAM contents and features; the extracted features are then numerically simulated and validated. This analysis is followed by a discussion of the extension to the multilayered fiber. The ramifications of the findings are explored in Section 4 for polarization corrections, leading to a general expression for a multilayered fiber (step-index or the three-layered ring-core fiber). This general expression includes the explicit impact of the polarization-induced field component. Analytic expressions specific to the step-index fiber are subsequently derived for illustrative purposes and numerically simulated. Section 5 is the summary and discussion.

2. General OAM composition of the vector fields in a fiber

We begin by writing the generic form of the vector fields expressed directly in the $e^{\pm il\theta}$ basis used in the solution of the vector wave equation:

$$\vec{e}^{(l)} = \left(e_r^{(l)}(r)\hat{r} + e_\theta^{(l)}(r)\hat{\theta} + e_z^{(l)}(r)\hat{z} \right) e^{il\theta}, \quad (5)$$

where l is an azimuthal parameter, and where we have assumed that the fiber is translationally invariant and the refractive index depends upon the radial distance r only, i.e., $n^2 = n^2(r)$. Noting that $\hat{r} = \hat{x} \cos \theta + \hat{y} \sin \theta$ and $\hat{\theta} = -\hat{x} \sin \theta + \hat{y} \cos \theta$, the transverse field comprised of the first two terms in Eq. 5 can be reexpressed as

$$\vec{e}_t^{(l)} = (1/\sqrt{2}) \left[\vec{\epsilon}_+ e^{i(l-1)\theta} (e_r^{(l)}(r) - i e_\theta^{(l)}(r)) + \vec{\epsilon}_- e^{i(l+1)\theta} (e_r^{(l)}(r) + i e_\theta^{(l)}(r)) \right], \quad (6)$$

where $\vec{\epsilon}_\pm = (1/\sqrt{2})(\hat{x} \pm i\hat{y})$ are left/right-circular polarizations associated with a spin angular momentum $S_z = \pm 1$ (left/right circularly polarized photons have spins $\pm\hbar$). Invoking the OAM operator, $L_z^{OP} = (1/i)(\partial/\partial\theta)$ [13], we observe that in the above field equation, spins of $S_z = +1$ and $S_z = -1$ are coupled with orbital angular momentum values of $L_z = \ell - 1$ and $L_z = \ell + 1$, respectively so the total angular momentum, denoted J_z , in each of the first two terms is $J_z = L_z + S_z = \ell$. Thus, the transverse fields may be regarded as the eigenstates of the total angular momentum operator J_z . The second term differs in topological charge by ± 2 . Changing l to $l \pm 1$ then yields

$$\vec{e}_t^{(l\pm 1)} = (1/\sqrt{2}) \left[\vec{\epsilon}_\pm e^{il\theta} (e_r^{(l\pm 1)}(r) \mp i e_\theta^{(l\pm 1)}(r)) + \vec{\epsilon}_\mp e^{i(l\pm 2)\theta} (e_r^{(l\pm 1)}(r) \pm i e_\theta^{(l\pm 1)}(r)) \right]. \quad (7)$$

Similar results are obtained for the associated magnetic field, denoted $\vec{h}_t^{(l\pm 1)}$:

$$\vec{h}_t^{(l\pm 1)} = (1/\sqrt{2}) \left[\vec{\epsilon}_\pm e^{il\theta} (h_r^{(l\pm 1)}(r) \mp i h_\theta^{(l\pm 1)}(r)) + \vec{\epsilon}_\mp e^{i(l\pm 2)\theta} (h_r^{(l\pm 1)}(r) \pm i h_\theta^{(l\pm 1)}(r)) \right]. \quad (8)$$

These solutions in conjunction with the z field components, $\vec{e}_z^{(l\pm 1)}$ and $\vec{h}_z^{(l\pm 1)}$, are identified with the familiar vector modes, HE_{l+1} and EH_{l-1} , expressed in the exponential basis [14].

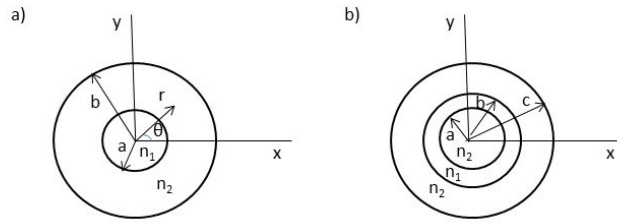


Fig. 1. a) Cross section of a step-index fiber with core radius a and cladding radius b ($\gg a$); n_1 and n_2 are the refractive indices of the core and cladding, respectively; r and θ along with the z coordinate (z axis coincident with the fiber axis) constitute the polar coordinates; the mode is assumed propagating in the $+z$ direction (out of the plane of the paper). b) Cross section of a ring core fiber, with refractive index n_1 for the ring core ($a \leq r \leq b$) and cladding refractive index equal to $n_2 < n_1$ in the fiber region: $0 \leq r \leq a$ and $b \leq r \leq c$ ($c \gg b$); in the limit $a \rightarrow 0$, we obtain the step-index fiber.

In what follows, we determine the exact forms of the two components in Eq. 7 for the step-index fiber and the ring-core fiber (see Fig. 1) using the analytic expressions for the radial and the azimuthal components of the electric fields. In particular, we study the OAM characteristics of the fields in a step-index fiber in detail.

3. OAM modal fields in a multilayered fiber

We consider the step-index fiber (two layers) first followed by an extension of the technique to more than two-layers.

3.1. Step-Index fiber

In a standard manner of solving for the fields within a step-index fiber [15], we consider the steady-state solutions: $\vec{E}^{(l)}(\vec{r}, t) = \vec{e}^{(l)}(r, \theta)e^{i(\beta_l z - \omega t)}$ and $\vec{H}^{(l)}(\vec{r}, t) = \vec{h}^{(l)}(r, \theta)e^{i(\beta_l z - \omega t)}$, where β_l is the propagation constant of the mode and $\omega = k/\sqrt{\epsilon_0\mu_0}$ is the angular frequency. We subsequently apply the Maxwell's equations, starting with $E_z^{(l)}(r, \theta) = e_z^{(l)}(r)e^{il\theta}$, where $e_z^{(l)}(r) = A_l J_l(p_l r)$, and $H_z^{(l)}(r, \theta) = h_z^{(l)}(r)e^{il\theta}$, where $h_z^{(l)}(r) = B_l J_l(p_l r)$, within the fiber core of radius a ; similarly, for the cladding region ($r \geq a$), we write $E_z^{(l)}(r, \theta) = e_z^{(l)}(r)e^{il\theta}$, where $e_z^{(l)}(r) = C_l K_l(q_l r)$, and $H_z^{(l)}(r, \theta) = h_z^{(l)}(r)e^{il\theta}$, where $h_z^{(l)}(r) = D_l K_l(q_l r)$. The results for the radial profiles, $e_r^{(l)}$ and $e_\theta^{(l)}$, comprising the transverse field (see Eq. 5) are

$$e_r^{(l)} = (i\beta_l/p_l^2) \left[A_l p_l J_l'(p_l r) + B_l (il/r)(\mu_0\omega/\beta_l) J_l(p_l r) \right], \quad (9)$$

$$e_\theta^{(l)} = (i\beta_l/p_l^2) \left[A_l (il/r) J_l(p_l r) - (\mu_0\omega p_l/\beta_l) B_l J_l'(p_l r) \right]; \quad r \leq a \quad (10)$$

$$e_r^{(l)} = -(i\beta_l/q_l^2) \left[C_l q_l K_l'(q_l r) + D_l (il/r)(\mu_0\omega/\beta_l) K_l(q_l r) \right], \quad (11)$$

$$e_\theta^{(l)} = -(i\beta_l/q_l^2) \left[C_l (il/r) K_l(q_l r) - (\mu_0\omega q_l/\beta_l) D_l K_l'(q_l r) \right]. \quad r \geq a \quad (12)$$

J_l and K_l are the Bessel and the modified Bessel functions, respectively. A_l, B_l, C_l, D_l are constants that are determined from matching the tangential components, $e_\theta^{(l)}, e_z^{(l)}, h_\theta^{(l)}, h_z^{(l)}$, at the interface $r = a$; $kn_2 \leq \beta_l \leq kn_1$; $p_l^2 = k^2 n_1^2 - \beta_l^2 (\geq 0)$; $q_l^2 = -(k^2 n_2^2 - \beta_l^2) (\geq 0)$; $k^2 = \omega^2 \mu_0 \epsilon_0$. Physically, p_l is the transverse component of the propagation constant (wave number), kn_1 , within the core medium, while β_l is the horizontal component, coincident with the z axis; parameter q_l has a similar interpretation, being the magnitude of the imaginary transverse component within the cladding, where the fields quickly decline to zero. For the fields within the core, we now find using the identities, $J_{l\pm 1}(x) = \mp J_l'(x) + (l/x)J_l(x)$, that

$$e_r^{(l)} \mp i e_\theta^{(l)} = \pm (i\beta_l/p_l) A_l J_{l\mp 1}(p_l r) \left(1 \pm (i\omega\mu_0/\beta_l)(B_l/A_l) \right), \quad (13)$$

and similarly for the fields within the cladding ($r \geq a$) we obtain

$$e_r^{(l)} \mp i e_\theta^{(l)} = (i\beta_l/q_l) C_l K_{l\mp 1}(q_l r) \left(1 \pm (i\omega\mu_0/\beta_l)(D_l/C_l) \right); \quad (14)$$

$D_l/C_l = B_l/A_l$ and $C_l/A_l = J_l(p_l a)/K_l(q_l a)$ [15].

3.1.1. Analysis of the $J = l + 1$ case

Changing l to $l + 1$ in Eq. 13 and inserting the resulting expressions in Eq. 7, we obtain for the fields within the core

$$\vec{e}_l^{(l+1)} = (1/\sqrt{2})(i\beta_{l+1}/p_{l+1}) A_{l+1} \left[\gamma_+^{(l+1)} J_l(p_{l+1} r) e^{il\theta} \vec{e}_+ + \gamma_-^{(l+1)} J_{l+2}(p_{l+1} r) e^{i(l+2)\theta} \vec{e}_- \right], \quad (15)$$

where

$$\gamma_{\pm}^{(l+1)} = \pm \left(1 \pm (i\omega\mu_0/\beta_{l+1})(B_{l+1}/A_{l+1}) \right), \quad (16)$$

and B_{l+1}/A_{l+1} is determined from the boundary conditions as discussed earlier.

Eq. 15 is a very general result, and a remarkable one because the spatial forms in Eq. 15 resemble the scalar field amplitudes (solutions of the scalar wave equation). Parameter p_{l+1} in the argument of the Bessel functions, J_l and J_{l+2} , is given by $p_{l+1}^2 = k^2 n_1^2 - \beta_{l+1}^2$. The corresponding counterpart \tilde{p}_l in the solution of the scalar wave equation, $\tilde{e}_l^{(l)} \sim J_l(\tilde{p}_l r) e^{il\theta} \tilde{e}_+$ (see Eq. 2), is similarly related by $\tilde{p}_l^2 = k^2 n_1^2 - \tilde{\beta}_l^2$. Consequently, $\tilde{p}_l^2 - p_{l+1}^2 = \beta_{l\pm 1}^2 - \tilde{\beta}_l^2 = \delta\beta_{l\pm 1}^2$, which is of order $\Delta \ll 1$ in WGA and therefore very small. Thus, p_{l+1} in the argument of J_l in Eq. 15 can be replaced with \tilde{p}_l , implying *we may identify the first term in Eq. 15 with the field of the traditional scalar OAM_l mode possessing a topological charge l and an amplitude $O_l(r, \theta) = J_l(\tilde{p}_l r) e^{il\theta}$ [1]* (see also Appendix A). Peak intensity defined as the square of the magnitude of O_l occurs at the first maximum of the $J_l(\tilde{p}_l r)$ function. If we define $r = r_{max}^{(l)}$ as this maximum, then $r_{max}^{(l)} = x_{max}/\tilde{p}_l$, where x_{max} is the first maximum of $J_l(x)$, $l > 0$. Since the Bessel function rises from its zero value with increase in its argument value, the intensity of this mode as a function of the radial distance r is the familiar donut pattern, often observed in experimental data (see, e.g, [5]).

The second term in Eq. 15, however, does not correspond to the field of the traditional scalar OAM_{l+2} mode because its radial profile, $J_{l+2}(p_{l+1}r) \approx J_{l+2}(\tilde{p}_l r)$ is not the same as the profile, $J_{l+2}(\tilde{p}_{l+2}r)$ of the traditional OAM_{l+2} scalar mode. This is due to the fact that $\tilde{p}_{l+2} \neq \tilde{p}_l$. In fact, $\tilde{p}_{l+2} > \tilde{p}_l$ (see Table 1) because $\tilde{\beta}_{l+2} < \tilde{\beta}_l$. As a result, the second term in Eq. 15 is a modified OAM_{l+2} modal field, whose predicted intensity maximum occurs at $r = r_{max}^{\prime(l+2)}$, where

Table 1. The second term in Eq. 15 is the field of a nontraditional (modified) scalar OAM_{l+2} mode, whose intensity maximum at the radial distance, $r_{max}^{\prime(l+2)}$ is shifted outward by a factor $f_l^+ = \tilde{p}_{l+2}/\tilde{p}_l$ relative to the position $r_{max}^{(l+2)}$ of the intensity maximum of the conventional scalar OAM_{l+2} mode; the numerical values are for a step-index fiber with parameters: $n_1 = 1.461$, $n_2 = 1.444$, $a = 25\mu\text{m}$, $\lambda = 1.55\mu\text{m}$ (see Fig. 1).

l	\tilde{p}_l	\tilde{p}_{l+2}	f_l^+	$r_{max}^{(l+2)}/a$	$r_{max}^{\prime(l+2)}/a$
1	3.6681	6.1063	1.66	0.69	1.15
2	4.9158	7.2617	1.48	0.73	1.08
3	6.1063	8.3927	1.37	0.76	1.04
4	7.2617	9.5056	1.31	0.79	1.03
5	8.3927	10.6043	1.26	0.81	1.02

$$r_{max}^{\prime(l+2)} = (\tilde{p}_{l+2}/\tilde{p}_l) r_{max}^{(l+2)}; \quad (17)$$

$r_{max}^{(l+2)}$ is the radial distance at which the intensity of the traditional OAM_{l+2} mode reaches its maximum. Because $\tilde{p}_{l+2} > \tilde{p}_l$, this maximum is shifted outward in the characteristic donut shaped intensity pattern, even beyond $r = a$ (see Table 1). However, because the fields drop off exponentially into the cladding region (being given by Eq. 14 for $r > a$), the maximum consequently occurs at $r = a$. The relatively low intensity region (the dark region of the donut), nevertheless, scales by a factor of $f_l^+ = \tilde{p}_{l+2}/\tilde{p}_l > 1$. Figure 2 shows the predicted intensity

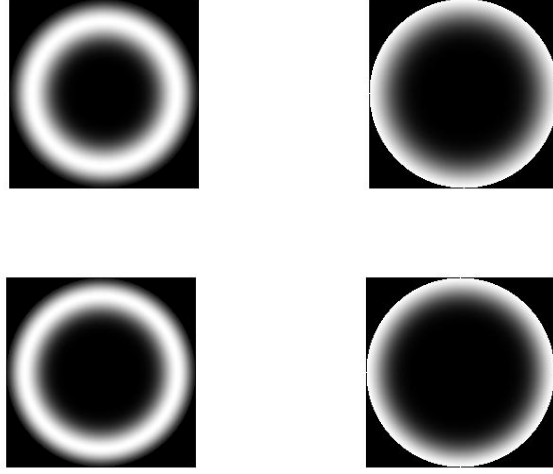


Fig. 2. The $J = l + 1$ case; the intensity pattern within the core, $J_{l+2}^2(\tilde{p}_{l+2}r)$, corresponding to the traditional scalar OAM_{l+2} mode (on the left) and the expanded out intensity pattern ($J_{l+2}^2(\tilde{p}_l r)$) corresponding to the modified scalar OAM_{l+2} modal field (on the right), as predicted by our theoretical expression (the second term in Eq. 15); see text for more details; the top row is for $l = 3$ and the bottom row is for $l = 5$ (see Table 1).

pattern (within the core) of the modified scalar OAM modal field (on the right) contrasted with the corresponding traditional scalar mode (on the left) for $l = 3$ (top row) and $l = 5$ (bottom row); the step-index fiber is described by $n_1 = 1.461$, $n_2 = 1.444$, core radius $a = 25 \mu\text{m}$; wavelength $\lambda = 1.55 \mu\text{m}$ is assumed.

3.1.2. Analysis of the $J = l - 1$ case

Changing l to $l - 1$ in Eq. 15 and substituting in Eq. 7, we obtain

$$\vec{e}_t^{(l-1)} = (1/\sqrt{2})(i\beta_{l-1}/p_{l-1})A_{l-1} \left[\gamma_+^{(l-1)} J_l(p_{l-1}r) e^{i l \theta} \vec{e}_- + \gamma_-^{(l-1)} J_{l-2}(p_{l-1}r) e^{i(l-2)\theta} \vec{e}_+ \right], \quad (18)$$

where

$$\gamma_{\pm}^{(l-1)} = \mp \left(1 \mp (i\omega\mu_0/\beta_{l-1})(B_{l-1}/A_{l-1}) \right). \quad (19)$$

The field corresponds to the EH_{l-1} mode. In WGA, $\beta_{l-1} \approx \tilde{\beta}_l$, the corresponding solution of the scalar wave equation (see Section 1); consequently, $p_{l-1} \approx \tilde{p}_l$. So, the first term corresponds to the traditional scalar mode with the radial profile, $J_l(\tilde{p}_l r)$, while the second term is a *modified* scalar modal field because the associated radial function, $J_{l-2}(p_{l-1}r) \approx J_{l-2}(\tilde{p}_l r)$, is different from $J_{l-2}(\tilde{p}_{l-2}r)$, the radial profile of the scalar OAM mode characterized by topological charge $l - 2$. The donut intensity pattern here has a radius

$$r_{max}^{(l-2)} = (\tilde{p}_{l-2}/\tilde{p}_l) r_{max}^{(l-2)}, \quad (20)$$

which is reduced since $\tilde{p}_{l-2} < \tilde{p}_l$, i.e., an intensity pattern as determined solely by the modified modal field, would be shifted inward towards the center by a factor $f_l^- \approx \tilde{p}_{l-2}/\tilde{p}_l$; see Table 2 and Figure 3; *the intensity pattern here displays the secondary maxima not present in the traditional scalar OAM_{l-2} fields.*

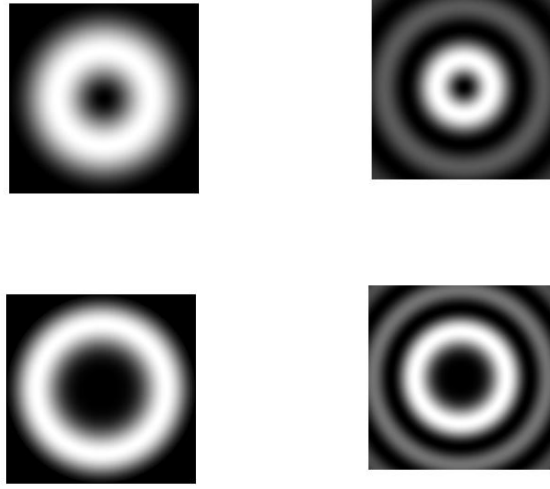


Fig. 3. The $J = l - 1$ case; the intensity pattern within the core, $J_{l-2}^2(\tilde{p}_l r)$, corresponding to the traditional scalar OAM_{l-2} mode (on the left) and the shrunken intensity pattern $J_{l-2}^2(\tilde{p}_{l-2} r)$ corresponding to the modified scalar OAM_{l-2} field (on the right), as predicted by our theoretical expression (the second term in Eq. 18); see text for more details; the top row is for $l = 3$ and the bottom row is for $l = 5$ (see Table 2).

Table 2. The second component in Eq. 15 is a nontraditional (modified) scalar OAM_{l-2} modal field, whose intensity maximum, $r_{max}^{\prime(l-2)}$ is shifted by a factor $f_l^- = \tilde{p}_{l-2}/\tilde{p}_l$; $r_{max}^{(l-2)}$ is the position of the intensity maximum of the conventional scalar OAM_{l-2} mode; the numerical values are for a step-index fiber with parameters: $n_1 = 1.461$, $n_2 = 1.444$, $a = 25\mu m$, $\lambda = 1.55\mu m$ (see Fig. 1).

l	\tilde{p}_l	\tilde{p}_{l-2}	f_l^-	$r_{max}^{(l-2)}/a$	$r_{max}^{\prime(l-2)}/a$
3	6.1063	3.6681	0.60	0.50	0.30
4	7.2617	4.9158	0.68	0.62	0.42
5	8.3927	6.1063	0.73	0.69	0.50
6	9.5056	7.2617	0.76	0.73	0.56
7	10.6043	8.3927	0.79	0.76	0.60

3.1.3. Relative amplitude of the modified scalar modal field

We need to evaluate the coefficients, $\gamma_{\pm}^{(l+1)}$ (see Eqs. 15 and 16) and $\gamma_{\pm}^{(l-1)}$ (see Eqs. 18 and 19). We first note that

$$\frac{B_l}{A_l} = \frac{il\beta_l}{\omega\mu_0} \left(\frac{1}{q_l^2 a^2} + \frac{1}{p_l^2 a^2} \right) \left(\frac{J_l'(p_l a)}{p_l a J_l(p_l a)} + \frac{K_l'(q_l a)}{q_l a K_l(q_l a)} \right)^{-1}, \quad (21)$$

which is easily derived from the boundary conditions at the core-cladding interface [15]. The characteristic equation for vector modes is well-known [2, 15]:

$$\left(n_1^2 \frac{J'_l(p_1 a)}{p_1 a J_l(p_1 a)} + n_2^2 \frac{K'_l(q_1 a)}{q_1 a K_l(q_1 a)}\right) \left(\frac{J'_l(p_1 a)}{p_1 J_l(p_1 a)} + \frac{K'_l(q_1 a)}{q_1 a K_l(q_1 a)}\right) = l^2 \left(\frac{1}{q_1^2 a^2} + \frac{1}{p_1^2 a^2}\right) \frac{\beta_l^2}{k^2}. \quad (22)$$

In the limit, $n_2 \rightarrow n_1$, the above characteristic equation reduces to the characteristic equation for the scalar modes [2, 15], assuming $\beta_l \approx kn_1$. In a real fiber, n_2 and n_1 are not exactly equal, being related by $n_2^2 = n_1^2(1 - 2\Delta)$, where Δ is usually a small fraction. Inserting this expression in Eq. 22 then leads to the following relationship:

$$\delta_l = \pm \frac{kn_1 \alpha_l}{\beta_l l} \left(1 - \frac{2\Delta \kappa_l}{\alpha_l}\right)^{1/2}, \quad (23)$$

where

$$\delta_l = \left(\frac{1}{q_1^2 a^2} + \frac{1}{p_1^2 a^2}\right), \quad (24)$$

$$\alpha_l = \left(\frac{J'_l(p_1 a)}{p_1 a J_l(p_1 a)} + \frac{K'_l(q_1 a)}{q_1 a K_l(q_1 a)}\right), \quad (25)$$

$$\kappa_l = \frac{K'_l(q_1 a)}{q_1 a K_l(q_1 a)}. \quad (26)$$

In terms of the above parameters, Eq. 21 can be rewritten as

$$\frac{B_l}{A_l} = \frac{il\beta_l}{\omega\mu_0} \left(\frac{\delta_l}{\alpha_l}\right), \quad (27)$$

which further upon substitution of Eq. 23 yields

$$\frac{B_l}{A_l} = \pm \frac{ikn_1}{\omega\mu_0} \left(1 - \frac{2\Delta \kappa_l}{\alpha_l}\right)^{1/2}. \quad (28)$$

This is a very general and exact result, regardless of the magnitude of Δ . Eq. 28, when substituted in Eq. 13, determines the complete analytic expressions for the electric field. The + sign corresponds to the EH_{l-1} mode and the negative sign to the HE_{l+1} mode. In the limit $\Delta \rightarrow 0$, $B_l/A_l = \pm ikn_1/(\omega\mu_0)$, which leads to the conventional scalar modal fields (see Appendix A).

$J = l + 1$

We change l to $l + 1$ in Eq. 28 and insert the resulting expression for B_{l+1}/A_{l+1} with a negative sign, in Eq. 16 to obtain

$$\gamma_+^{(l+1)} = 1 + \frac{kn_1}{\beta_{l+1}} \left(1 - \frac{2\Delta \kappa_{l+1}}{\alpha_{l+1}}\right)^{1/2}, \quad (29)$$

$$\gamma_-^{(l+1)} = -1 + \frac{kn_1}{\beta_{l+1}} \left(1 - \frac{2\Delta \kappa_{l+1}}{\alpha_{l+1}}\right)^{1/2}. \quad (30)$$

When $\Delta \ll 1$ (e.g., $\Delta \approx 0.01$ in a standard commercial multimode step-index fiber and ≈ 0.02 in considered ring-core fibers [6, 7]), we can expand Eqs. 29 and 30 to first order in Δ ; further, using the fact that $\beta_{l+1} \approx kn_1$, we arrive at

$$\gamma_+^{(l+1)} = 2 - \Delta \left(\frac{\kappa_{l+1}}{\alpha_{l+1}} \right) \quad (31)$$

and

$$\gamma_-^{(l+1)} = -\Delta \left(\frac{\kappa_{l+1}}{\alpha_{l+1}} \right), \quad (32)$$

leading to the relative amplitude

$$\mu_{l+1} = \gamma_-^{(l+1)} / \gamma_+^{(l+1)} = -\Delta \left(\frac{\kappa_{l+1}}{2\alpha_{l+1}} \right) \quad (33)$$

to first order in Δ . Eq. 33 provides the relative strength of the modified scalar modal field, which we find to be of order Δ in the first order correction; this is consistent with the expansion of the electric field in terms of Δ in [2]. This modified scalar modal field is the *polarization-induced* component of the vector field [10], as discussed in Section 1. Insertion of Eqs. 31 and 33 in Eq. 15 then provides a complete description of the transverse vector OAM field in terms of its two components differing in topological charge by 2. The parameters p_{l+1} and q_{l+1} in the expressions for κ_{l+1} and α_{l+1} correspond to the vector mode solution, HE_{l+1} . The two components in Eq. 15 move as one entity (in conjunction with the z component, which is very small; see Appendix A) with a propagation constant β_{l+1} corresponding to the HE_{l+1} vector mode. In other words, the polarization-induced field, the second component, which has the same propagation constant β_{l+1} as the first (primary) component, must have the same value $p_{l+1} (\approx \tilde{p}_l$ in WGA) as the primary component, and not \tilde{p}_{l+2} , which is characteristic of the traditional scalar mode of topological charge $l + 2$ in WGA.

$J = l - 1$

Here we change l to $l - 1$ in Eq. 28 and insert the resulting expression (with the positive sign) in Eq. 19. This yields the following expressions:

$$\gamma_+^{(l-1)} = -1 - \frac{kn_1}{\beta_{l+1}} \left(1 - \frac{2\Delta\kappa_{l+1}}{\alpha_{l+1}} \right)^{1/2}, \quad (34)$$

$$\gamma_-^{(l-1)} = 1 - \frac{kn_1}{\beta_{l+1}} \left(1 - \frac{2\Delta\kappa_{l+1}}{\alpha_{l+1}} \right)^{1/2}. \quad (35)$$

Retaining the first term in the binomial expansion of Eqs. 34 and 35 in $\Delta (\ll 1)$, and using the fact that $\beta_{l-1} \approx kn_1$, we arrive at

$$\gamma_+^{(l-1)} = -2 + \Delta \left(\frac{\kappa_{l+1}}{\alpha_{l+1}} \right) \quad (36)$$

and

$$\gamma_-^{(l-1)} = \Delta \left(\frac{\kappa_{l+1}}{\alpha_{l+1}} \right), \quad (37)$$

which implies that the relative polarization-induced field coefficient, denoted μ_{l-1} , here is given by

$$\mu_{l-1} = \gamma_-^{(l-1)} / \gamma_+^{(l-1)} = -\Delta \left(\frac{\kappa_{l-1}}{2\alpha_{l-1}} \right); \quad (38)$$

parameters p_{l-1} and q_{l-1} , occurring in κ_{l-1} and α_{l-1} , correspond to the solution EH_{l-1} , which has a different characteristic equation than that of the corresponding HE_{l-1} mode [2]. Insertion of Eqs. 36 and 38 in Eq. 18 now yields a complete description of the contribution of the polarization-induced component. This polarization-induced component of topological charge $l - 2$ moves with the same propagation constant β_{l-1} as the primary component (which is the field of a traditional scalar mode in WGA), and therefore is characterized by $p_{l-1} \approx \tilde{p}_l$, and not \tilde{p}_{l-2} , the parameter corresponding to the traditional scalar mode of topological charge $l - 2$.

3.2. Numerical validation

Here we compare the exact solution of the vector wave equation with the results derived on the basis of $\Delta \ll 1$; in the latter case, we recast the results in terms of the solutions of the scalar wave equation. Consequently, focusing first on the $J = l + 1$ case, we insert Eqs. 31 and 32 (or 33) into Eq. 15, and set $\beta_{l+1} \approx \tilde{\beta}_l$, $p_{l+1} \approx \tilde{p}_l$, and $q_{l+1} \approx \tilde{q}_l$, results valid in WGA. Subsequently, we arrive at

$$|\vec{e}_t^{(l+1)}|^2 = 2(\tilde{\beta}_l/\tilde{p}_l)^2 |A_{l+1}|^2 (1 - \Delta \tilde{\kappa}_{l+1}/(2\tilde{\alpha}_{l+1}))^2 \left[J_l^2(\tilde{p}_l r) + \frac{\Delta^2 \tilde{\kappa}_l^2}{4\tilde{\alpha}_l^2} J_{l+2}^2(\tilde{p}_l r) \right], \quad (39)$$

which, apart from the constant, A_{l+1}^2 , is an expression given entirely in terms of the scalar parameters (the second term is the contribution of the polarization-induced component). This expression is to be contrasted with the expression

$$|\vec{e}_t^{(l+1)}|^2 = |e_r^{(l+1)}|^2 + |e_\theta^{(l+1)}|^2, \quad (40)$$

where $e_r^{(l+1)}$ and $e_\theta^{(l+1)}$ represent the exact vector wave equation solutions given by Eqs. 9 and 10, but with l replaced with $l + 1$. We now define $I_S^{(l+1)} = \int_0^a \int_0^{2\pi} |\vec{e}_t^{(l+1)}|^2 r dr d\theta = 2\pi \int_0^a |\vec{e}_t^{(l+1)}|^2 r dr$, which is representative of the intensity of the field; a is the radius of the fiber core (where most light energy resides) and $|\vec{e}_t^{(l+1)}|^2$ is given by Eq. 39. Similarly, we write $I_V^{(l+1)} = \int_0^a \int_0^{2\pi} |\vec{e}_t^{(l+1)}|^2 r dr d\theta = 2\pi \int_0^a |\vec{e}_t^{(l+1)}|^2 r dr$, where $|\vec{e}_t^{(l+1)}|^2$ is given by Eq. 40. For the $J = l - 1$ case, we use Eqs. 36 and 37 (or 38), in Eq. 18, which yields the same expression as in Eq. 39, except that the subscript $l + 1$ is replaced with $l - 1$ and subscript $l + 2$ is replaced with $l - 2$. We similarly define $I_S^{(l-1)}$ and $I_V^{(l-1)}$.

Table 3. $I_V^{(J)} = I_V/(2\pi|A_J|^2)$ and $I_S^{(J)} = I_S/(2\pi|A_J|^2)$ for the $J = l \pm 1$ cases and various values of topological charge l ; the percentage difference (fourth column), defined as $(I_V^{(J)} - I_S^{(J)})/I_V^{(J)} \times 100$, is of the order of 0.1 or less in magnitude (see text for more details); $n_1 = 1.461$, $n_2 = 1.444$, $a = 25\mu\text{m}$, $\lambda = 1.55\mu\text{m}$.

l	$I_V^{(l+1)}$	$I_S^{(l+1)}$	%diff	l	$I_V^{(l-1)}$	$I_S^{(l-1)}$	%diff
2	113.300575	113.476040	-0.15	2	115.246009	115.372053	-0.11
3	56.538155	56.611168	-0.13	3	57.383678	57.424266	-0.07
4	32.310729	32.342199	-0.10	4	32.797496	32.805129	-0.02
5	20.196714	20.208784	-0.06	5	20.5140336	20.507828	0.03

For our calculations done in MATLAB in double precision, we consider a multimode fiber with the same parameters as those used in Tables 1 and 2. Table 3 shows the results of numerical integration done for $I_V^{(J)}$ and $I_S^{(J)}$, where $J = l \pm 1$; for the former, we used two different characteristic equations, one corresponding to the HE_{l+1} modes and the other to the EH_{l-1} modes, while for $I_S^{(J)}$, we used the single characteristic equation corresponding to the scalar modes [2]. The differences (fourth table column) are of the order of a tenth percent or less, corroborating the veracity of our results expressed in terms of the scalar parameters. Furthermore, we observed that, using parameter \tilde{p}_{l+2} , instead of \tilde{p}_l , in the argument of J_{l+2} in Eq. 39, causes %diff in Table 3 (for the $l + 1$ case) to increase by a factor of 2 to 9 in magnitude, supporting the fact that the polarization-induced component of the electric field is indeed the field of a

modified scalar OAM mode of topological charge $l + 2$ as described in Section 3.1, and not the field of a traditional scalar mode of the same topological charge. Similar worsening of the results (although less dramatic) occurs in the $J = l - 1$ case, when \bar{p}_l in the argument of the Bessel function, J_{l-2} , is replaced with \bar{p}_{l-2} .

3.3. Extension to a multilayered fiber

In extending the above theoretical concepts to a cylindrical waveguide with more than two layers, we observe that, within each layer of the waveguide, the field solutions are, in general, a linear combination of the Bessel functions: $J_l(\alpha_i r)$ and $Y_l(\alpha_i r)$, when $\alpha_i^2 = (k^2 n_i^2 - \beta^2)$ is positive, and a linear combination of the modified Bessel functions: $I_l(\alpha_i r)$ and $K_l(\alpha_i r)$, when α_i^2 is negative. For the 3-layer fiber, defined by a ring core of radii a and $b (> a)$, refractive index n_1 , and inner and outer cladding refractive index of $n_2 < n_1$ (Fig. 1), the z component of the field is expressible in the azimuthal exponential basis as

$$\begin{aligned} e_z^{(l)} &= A_1^{(l)} I_l(q_1 r) e^{il\theta} \quad (r \leq a), \\ &= [C_1^{(l)} J_l(p_1 r) + C_2^{(l)} Y_l(p_1 r)] e^{il\theta} \quad (a \leq r \leq b), \\ &= A_2^{(l)} K_l(q_1 r) e^{il\theta} \quad (r \geq b); \end{aligned} \quad (41)$$

note that the fields within the cladding region die out. Similarly,

$$\begin{aligned} h_z^{(l)} &= B_1^{(l)} I_l(q_1 r) e^{il\theta} \quad (r \leq a), \\ &= [D_1^{(l)} J_l(p_1 r) + D_2^{(l)} Y_l(p_1 r)] e^{il\theta} \quad (a \leq r \leq b), \\ &= B_2^{(l)} K_l(q_1 r) e^{il\theta} \quad (r \geq b). \end{aligned} \quad (42)$$

Within the ring, $a \leq r \leq b$, where the fields are primarily concentrated, we obtain, using Maxwell's equations (as in the step-index fiber case) and the appropriate Bessel function recursion relations, the following expression:

$$\begin{aligned} e_r^{(l)} \mp i e_\theta^{(l)} &= (i\beta_l / p_l) C_1^{(l)} [(\pm J_{l\mp 1}(p_1 r) (1 \pm (i\mu_0 \omega / \beta) (D_1^{(l)} / C_1)) \\ &\quad \pm C_2^{(l)} / C_1^{(l)} (1 \pm (i\mu_0 \omega / \beta) (D_2^{(l)} / C_2^{(l)}) Y_{l\mp 1}(p_1 r))]; \end{aligned} \quad (43)$$

the ratios, $D_1^{(l)} / C_1^{(l)}$, $C_2^{(l)} / C_1^{(l)}$, $D_2^{(l)} / C_2^{(l)}$ are determined from the boundary conditions at the two interfaces, $r = a$ and $r = b$. Changing l to $l + 1$ and inserting the resulting expression in Eq. 7, for the $l + 1$ case the first term is the linear combination of $J_l(p_{l+1} r)$ and $Y_l(p_{l+1} r)$ coupled with polarization $\tilde{\epsilon}_+$ and the second term is the linear combination of $J_{l+2}(p_{l+1} r)$ and $Y_{l+2}(p_{l+1} r)$ coupled with polarization $\tilde{\epsilon}_-$. This is very similar to the expression, Eq. 15, for the step-index fiber. A detailed analysis, as in the step-index fiber, is cumbersome (as is also seen in [6]) and not done here. However, we note that the fields are confined within the ring and, intuitively, similar conclusions would hold as in the step-index fiber, to which the ring-core fiber reduces in the limit $a \rightarrow 0$; for thin rings, however, the changes in the radius of the annular bright intensity ring would accordingly be small.

4. General form of the polarization correction

In this section, we evaluate the impact of the second component (the modified scalar modal field) on the polarization correction to the propagation constant of a scalar mode. Prior work [2, 8–10] has not considered it, partly due to the lack of an analytic expression as discussed in Section 1.

We first derive a generic form for polarization correction of propagation constant in a multilayered

fiber. This form includes the explicit contribution of the polarization-induced component (the second component) in Eq. 7. We also assume the WGA so that we can write the polarization-induced field correction (see Eq. 4 and Eq. 7) as

$$\delta \vec{e}_t^{(l\pm 1)} = G_{l\pm 2}(r) e^{i(l\pm 2)\theta} \vec{e}_\mp. \quad (44)$$

For multilayered fibers such as the step-index fiber and the three-layer ring-core fiber, characterized by a core refractive index of n_1 and a cladding refractive index of n_2 (see Fig. 1), the function $G_{l\pm 2}(r) = G_{l\pm 2}(p_{l+1}r)$, where the parameter $p_{l+1}^2 = k^2 n_1^2 - \beta_{l+1}^2$. Recalling $\vec{e}_t^{(l)} = F_l(r) e^{il\theta} \vec{e}_\pm$, we substitute $\vec{e}_t^{(l\pm 1)} = \vec{e}_t^{(l)} + \delta \vec{e}_t^{(l\pm 1)}$ into Eq. 1. After taking scalar products and performing the necessary integrations (see Appendix B), we arrive at the general form for *polarization correction*

$$\begin{aligned} \delta \beta_{l\pm 1}^2 &= \beta_{l\pm 1}^2 - \tilde{\beta}_l^2 \\ &= -\pi \left[\int_0^\infty \frac{\partial(\ln(n^2))}{\partial r} F_l \left(\frac{dF_l(r)}{dr} \mp \frac{l}{r} F_l \right) r dr + \int_0^\infty \frac{\partial \ln(n^2)}{\partial r} G_{l\pm 2} \left(\frac{dF_l(r)}{dr} \mp \frac{l}{r} F_l \right) r dr \right]. \end{aligned} \quad (45)$$

The radial amplitudes, $F_l(r)$ and $G_{l\pm 2}(r)$, are characteristic of the multilayered fiber under consideration. The first integral is identified with the familiar polarization correction [2, 8, 10]; *the second integral is the correction due to the polarization-induced field component*. Furthermore, Δ being less than one allows us to make an expansion of $\ln(n^2)$ in the parameter Δ (Section 1). The function $G_{l\pm 2}$ in the second term of Eq. 45 is of order Δ , so an expansion of $\ln(n^2)$ to first order in Δ yields a result quadratic in Δ .

4.1. Expression valid up to second order in Δ

To obtain the expression valid up to second order in $\Delta \ll 1$, we note that $n^2 = n_1^2(1 - 2\Delta f(r))$ and use the expansion, $\ln(1 - x) = -x - x^2/2 + \dots$ in Eq. 45 to arrive at

$$\delta \beta_{l\pm 1}^2 = \frac{2\pi\Delta}{N_l} \left[\int_0^\infty (1+2\Delta f(r)) \frac{\partial f(r)}{\partial r} F_l \left(\frac{dF_l(r)}{dr} \mp \frac{l}{r} F_l \right) r dr + \int_0^\infty \frac{\partial f(r)}{\partial r} G_{l\pm 2} \left(\frac{dF_l(r)}{dr} \mp \frac{l}{r} F_l \right) r dr \right]. \quad (46)$$

If we ignore the second term and replace $1 + 2\Delta f(r)$ by unity in Eq. 46, we obtain the result in [2, 10], which is the correction to first order in Δ . We consider now, for illustrative purposes, the step-index fiber.

4.2. Application to a step-index fiber

$n^2 = n_1^2(1 - 2\Delta f(r))$, where $\Delta \ll 1$. As a consequence, to first order in Δ , $\partial \ln(n^2)/\partial r = -2\Delta \partial f(r)/\partial r = -2\Delta \delta(r - a)$, the last step following from the fact that $f(r)$ is step function at $r = a$. Therefore, Eq. 46 reduces to

$$\delta \beta_{l\pm 1}^2 = \frac{2\pi\Delta}{N_l} \left[(1 + 2\Delta f(a)) F_l(F_l'(a) \mp \frac{l}{a} F_l(a)) a + G_{l\pm 2}(a) \left((F_l'(a) \mp \frac{l}{a} F_l(a)) a \right) \right], \quad (47)$$

where $F_l'(a)$ is $\partial F_l(r)/\partial r$ evaluated at $r = a$. Furthermore, as noted in the previous section,

$$F_l = (1/\sqrt{N_l}) J_l(\tilde{p}_l r), \quad (48)$$

$$G_{l\pm 2} = \mu_{l\pm 1} (1/\sqrt{N_l}) J_{l\pm 2}(\tilde{p}_l r), \quad (49)$$

where we have introduced a normalization constant, $N_l = 2\pi \int_0^\infty F_l^2(r) r dr$, and $\mu_{l\pm 1}$ represents the relative amplitude of the second component given by the expression in Eqs. 33 and 38. Substituting these expressions for $F_l(r)$ and $G_{l\pm 2}(r)$ in Eq. 47, and setting $f(a) = 1/2$, the

(mean) value of the step function at $r = a$, the polarization correction to second order in Δ for the step-index fiber is found to be

$$\delta\beta_{l\pm 1}^2 = \mp(2\pi\Delta/N_l)\left[(1 + \Delta)\tilde{p}_l a J_l(\tilde{p}_l a) J_{l\pm 1}(\tilde{p}_l a) + \mu_{l\pm 1} \tilde{p}_l a J_{l\pm 2}(\tilde{p}_l a) J_{l\pm 1}(\tilde{p}_l a)\right]. \quad (50)$$

$\mu_{l\pm 1} = -(1/2)\Delta(\kappa_{l\pm 1}/\alpha_{l\pm 1})$, $\kappa_{l\pm 1} = -K_l(\tilde{q}_l a)/(\tilde{q}_l a K_{l\pm 1}(\tilde{q}_l a)) \mp (l + 1)/(\tilde{q}_l a)^2$ and $\alpha_{l\pm 1} = \pm J_l(\tilde{p}_l a)/(\tilde{p}_l a J_{l\pm 1}(\tilde{p}_l a)) \mp (l \pm 1)/(\tilde{p}_l a)^2 \pm \kappa_{l\pm 1}$; we have used the fact that $p_{l\pm 1} \approx \tilde{p}_l$ and $q_{l\pm 1} \approx \tilde{q}_l$ and the appropriate Bessel function identities. The first term on the RHS of Eq. 50 is the contribution of the first integral in Eq. 46 up to second order in Δ (without the $1 + \Delta$ factor, it is the correction to first order in Δ [10]). The second term in Eq. 50 is of order Δ^2 and represents the impact of the polarization induced OAM field. From Eq. 50, $\delta\beta_{l\pm 1} = \delta\beta_{l\pm 1}^2/(2\beta_{l\pm 1}) \approx \delta\beta_{l\pm 1}^2/(2\tilde{\beta}_l)$ follows.

4.3. Numerical results

For numerical simulation we chose the multimode step-index fiber with parameters: $n_1 = 1.461$, $n_2 = 1.444$, $a = 25\mu m$, and $\lambda = 1.55\mu m$. The index profile height parameter $\Delta = 0.011568$. We first calculated $\delta\beta_{l+1}^{(CE)} = \beta_{l+1} - \tilde{\beta}_l$ and $\delta\beta_{l-1}^{(CE)} = \beta_{l-1} - \tilde{\beta}_l$, where β_{l+1} and β_{l-1} were determined from the characteristic equations for the HE_{l+1} and the EH_{l-1} modes, respectively, while the propagation constant, $\tilde{\beta}_l$ was determined from the characteristic equation for the scalar modes [2]. Values are displayed in Table 4 for $l = 2$ to $l = 5$. $\delta\beta_{l\pm 1}$, calculated directly from Eq. 50, is in agreement with the characteristic equation-based values $\delta\beta_{l\pm 1}^{(CE)}$ within a fraction of a percent. The fifth column is the contribution of the polarization-induced OAM component, denoted $\delta\beta_{l\pm 1}^{(P)}$, which is calculated from the second term in Eq. 50. It is observed to be about 1% of the total, which is of the order of Δ , as expected. The fractional differences (in column 4) are likely due to higher order terms not considered here All numerical calculations were done in MATLAB in double precision.

Table 4. Polarization corrections, $\delta\beta_{l\pm 1}^{(CE)}$ (in units of $meter^{-1}$) as calculated from the characteristic equations [2], and $\delta\beta_{l\pm 1}$ as calculated directly from the analytic expression, Eq. 50; the differences are of the order of a tenth of a percent; the fifth column is the contribution of the second term in Eq. 50.

l	$\delta\beta_{l+1}^{(CE)}$	$\delta\beta_{l+1}$	%diff	$\delta\beta_{l+1}^{(P)}$
2	-3.50859	-3.50404	0.13	0.03716
3	-5.59284	-5.58343	0.17	0.05935
4	-8.15965	-8.14574	0.17	0.08669
5	-11.22993	-11.20679	0.21	0.11944

l	$\delta\beta_{l-1}^{(CE)}$	$\delta\beta_{l-1}$	%diff	$\delta\beta_{l-1}^{(P)}$
2	-2.91831	-2.91505	0.11	0.04907
3	-4.25156	-4.24659	0.12	0.06203
4	-5.64576	-5.63868	0.13	0.07642
5	-7.04443	-7.03481	0.14	0.08994

4.4. Extension to ring-core fiber

A similar calculation can also be carried out for the ring-core-fiber (see Fig. 1) once the function $G_{l\pm 2}(r)$ has been extracted from the expression, Eq. 43; the refractive index function here is given by $n^2(r) = n_1^2(1 - 2\Delta f(r))$, where $f(r) = g(r - a) + h(r - b)$; $g(r - a) = 1$ for $r < a$ and equal to zero for $r \geq a$, and $h(r - b) = 1$ for $r \geq b$ and equal to zero for $r < b$. For $\partial f(r)/\partial r$ needed in Eq. 46, we note here that $\partial h(r - b)/\partial r = \delta(r - b)$ and $\partial g(r - a)/\partial r = -\delta(r - a)$.

5. Summary and discussion

We have critically investigated the nature of the transverse OAM fields in a multilayered cylindrical waveguide. In particular, in a detailed study of the step-index fiber (two-layered fiber), we have identified the polarization-induced component of the vector modal field as a modified scalar OAM mode, a hitherto unknown result. The intensity peak of this nontraditional OAM mode occurs at a larger or smaller radial distance in the characteristic donut intensity pattern, depending upon whether the spin is aligned with OAM or antialigned with OAM as in the transverse fields of the HE_{l+1} or the EH_{l-1} mode, respectively. An extension to other multilayered fibers such as the ring-core fiber shows the modified scalar field as a general feature of the polarization-induced component. The amplitude of this modified scalar mode is of order Δ , the index profile height parameter; thus larger the value of Δ , larger this amplitude. We also have developed analytic expressions for the contribution of this component to polarization correction, not done before. Specifically, we have applied these expressions to the case of a step-index fiber to illustrate their impact numerically. Such expressions along with the insight they provide can be useful in the analysis and design of fibers. Note also that, while the treatment here pertains to the multilayered fibers, the result of a polarization-induced component being a modified scalar modal field is a generic result that will manifest in any type of fiber (graded-index, or otherwise), simply because $\tilde{p}_l \neq \tilde{p}_{l\pm 2}$ in general.

Appendix

A. Reduction of the vector OAM modes to their scalar forms for the step-index fiber in weakly guiding approximation (WGA)

We first note that setting $n_2 = n_1$ and $\beta_l = kn_1$ in the characteristic equation for the vector modes (Eq. 22) yields

$$\frac{J'_l(p_l a)}{p_l a J_l(p_l a)} + \frac{K'_l(q_l a)}{q_l a K_l(q_l a)} = \pm |l| \left[\frac{1}{q_l^2 a^2} + \frac{1}{p_l^2 a^2} \right], \quad (51)$$

where the + sign corresponds to the EH_l mode and the - sign to the HE_l mode. Using the identities: $J'_l(x) = -J_{l+1}(x) + (l/x)J_l(x)$ and $K'_l(x) = -K_{l+1}(x) + (l/x)K_l(x)$ for the case of the + sign, and the identities: $J'_l(x) = J_{l-1}(x) - (l/x)J_l(x)$ and $K'_l(x) = -K_{l-1}(x) - (l/x)K_l(x)$ for the - sign, it can then be shown that the characteristic equation for EH_{l-1} mode and the characteristic equation for the HE_{l+1} mode coalesce into a single characteristic equation given by

$$\frac{J_l(\tilde{p}_l a)}{\tilde{p}_l a J_{l-1}(\tilde{p}_l a)} = -\frac{K_l(\tilde{q}_l a)}{\tilde{q}_l a K_{l-1}(\tilde{q}_l a)}, \quad (52)$$

where $\tilde{p}_l = p_{l+1}$ (HE modes) = p_{l-1} (EH modes) in the limit $n_1 \rightarrow n_2$. This is a form commonly found in literature in the context of LP modes [2, 15, 16].

We now note that the expression for B_l/A_l given in Eq. 21 reduces, upon substitution of Eq. 51, to

$$\frac{B_l}{A_l} = \pm \frac{i\beta_l}{\omega\mu_0}. \quad (53)$$

Eqs. 9 and 10 can be recast as

$$e_r^{(l)} = \frac{i\beta_l}{p_l^2} A_l \left[p_l J_l'(p_l r) + \frac{B_l}{A_l} (il) \left(\frac{\mu_0 \omega}{\beta_l r} \right) J_l(p_l r) \right], \quad (54)$$

$$e_\theta^{(l)} = \frac{i\beta_l}{p_l^2} A_l \left[\frac{il}{r} A_l J_l'(p_l r) - \frac{B_l}{A_l} \frac{\mu_0 \omega p_l}{\beta_l} J_l'(p_l r) \right]. \quad (55)$$

EH modes

Inserting Eq. 53 with the + sign and invoking the identity: $J_l'(x) = -J_{l+1}(x) + \frac{l}{x} J_l(x)$, one arrives at

$$e_r^{(l)} = A_l' J_{l+1}(p_l r), \quad (56)$$

$$e_\theta^{(l)} = (-i) A_l' J_{l+1}(p_l r), \quad (57)$$

where the constant A_l' is given by

$$A_l' = \left(\frac{-i\beta_l}{p_l} \right) A_l. \quad (58)$$

Now $\beta_l/p_l \gg 1$ because $p_l = (k^2 n_1^2 - \beta_l^2)^{1/2}$ is very small compared to $\beta_l \approx kn_1$. Consequently, $e_z^{(l)} = A_l J_l(p_l r)$ is very small compared to $e_r^{(l)}$ and $e_\theta^{(l)}$, and thus neglected generally. Note that $e_r^{(l)}$ and $e_\theta^{(l)}$ have the same magnitude but differ in phase by $\pi/2$. Substituting Eqs. 55 and 56 in Eq. 6, we obtain

$$\vec{e}_i^{(l)} = \sqrt{2} A_l' J_{l+1}(p_l r) e^{i(l+1)\theta} \vec{e}_-. \quad (59)$$

Changing $l \rightarrow l-1$,

$$\vec{e}_i^{(l-1)} = \sqrt{2} A_l' J_l(p_{l-1} r) e^{il\theta} \vec{e}_-, \quad (60)$$

which can be rewritten as

$$\vec{e}_i^{(l-1)} = \sqrt{2} A_l' O_l \vec{e}_-, \quad (61)$$

where

$$O_l = J_l(p_{l-1} r) e^{il\theta} = J_l(\tilde{p}_l r) e^{il\theta}; \quad (62)$$

O_l is the amplitude of the scalar OAM mode with topological charge l ; it is the solution of the scalar wave equation (Eq. 2) to which the vector wave equation (Eq. 1) reduces in the limit $\Delta \rightarrow 0$; parameter $\tilde{p}_l^2 = k^2 n_1^2 - \beta_l^2$. Eq. 61 signifies a field with a total angular momentum $J = L + S = l - 1$, since the polarization \vec{e}_- corresponds to a spin $S = -1$. It is a case of *spin-OAM nonalignment*.

HE modes

Taking the negative sign in Eq. 53, and following the same steps as for the EH mode, but invoking the identity: $J_l'(x) = J_{l-1}(x) - \frac{l}{x} J_l(x)$, one arrives at

$$e_r^{(l)}(r) = -A_l' J_{l-1}(p_l r) \quad (63)$$

and

$$e_\theta^{(l)}(r) = -i A_l' J_{l-1}(p_l r), \quad (64)$$

with $e_z^{(l)} \ll e_r^{(l)}, e_\theta^{(l)}$ in magnitude. Inserting the above expressions in Eq. 6, we obtain

$$\vec{e}_i^{(l)} = -\sqrt{2} A_l' J_{l-1}(p_l r) e^{i(l-1)\theta} \vec{e}_+, \quad (65)$$

which implies further

$$\vec{e}_t^{(l+1)} = -\sqrt{2}A'_{l+1}J_l(p_{l+1}r)e^{il\theta}\vec{e}_+ = -\sqrt{2}A'_{l+1}J_l(\tilde{p}_l r)e^{il\theta}\vec{e}_+. \quad (66)$$

Here the total angular momentum $J = L + S = l + 1$, i.e., we have a mode with *spin-OAM alignment*; $J_l(\tilde{p}_l r)e^{il\theta}$ is the scalar spatial OAM amplitude O_l .

B. Derivation of the general expression for polarization correction

The transverse vector field can be written in the weakly guiding approximation (WGA) as (see Eq. 4)

$$\vec{e}_t^{(l\pm 1)} = \vec{e}_t^{(l)} + \delta\vec{e}_t^{(l\pm 1)}, \quad (67)$$

where $\vec{e}_t^{(l)}$ is the corresponding scalar field and $\delta\vec{e}_t^{(l\pm 1)}$, the polarization-induced field, can be expressed as

$$\delta\vec{e}_t^{(l\pm 1)} = G_{l\pm 2}(r)e^{i(l\pm 2)\theta}\vec{e}_\mp. \quad (68)$$

Substituting Eq. 67 in Eq. 1 and invoking Eq. 2, we obtain

$$(\vec{\nabla}_t^2 + k^2 n^2)\delta\vec{e}_t^{(l\pm 1)} + \vec{\nabla}_t(\vec{e}_t^{(l\pm 1)} \cdot \vec{\nabla}_t \ln n^2) = \beta_{l\pm 1}^2 \delta\vec{e}_t^{(l\pm 1)} + \delta\beta_{l\pm 1}^2 \vec{e}_t^{(l)}, \quad (69)$$

where $\delta\beta_{l\pm 1}^2 = \beta_{l\pm 1}^2 - \tilde{\beta}_l^2$ (see Eq. 3). Now $G_{l\pm 2}(r) = G_{l\pm 2}(p_{l\pm 1}r)$, where the parameter $p_{l\pm 1}$ is given by $p_{l\pm 1}^2 = k^2 n_1^2 - \beta_{l\pm 1}^2$. Furthermore, the function $G_{l\pm 2}(p_{l\pm 1}r)$ is the Bessel functions $J_{l\pm 2}(p_{l\pm 1}r)$ for the step index fiber and a linear combination of $J_{l\pm 2}(p_{l\pm 1}r)$ and $Y_{l\pm 2}(p_{l\pm 1}r)$ for the ring-core fiber. Noting these facts it then follows from a direct substitution of Eq. 68 that

$$(\vec{\nabla}_t^2 + k^2 n^2)\delta\vec{e}_t^{(l\pm 1)} = (k^2 n_1^2 - p_{l\pm 1}^2)\delta\vec{e}_t^{(l\pm 1)} = \beta_{l\pm 1}^2 \delta\vec{e}_t^{(l\pm 1)}. \quad (70)$$

Inserting Eq. 70 into Eq. 69 yields

$$\delta\beta_{l\pm 1}^2 \vec{e}_t^{(l)} = \vec{\nabla}_t(\vec{e}_t^{(l\pm 1)} \cdot \vec{\nabla}_t \ln n^2) \quad (71)$$

leading to

$$\delta\beta_{l\pm 1}^2 = \langle \vec{e}_t^{(l)} | \vec{\nabla}_t(\vec{e}_t^{(l\pm 1)} \cdot \vec{\nabla}_t \ln n^2) \rangle = \int_0^\infty \int_0^{2\pi} \vec{e}_t^{(l)*} \cdot \vec{\nabla}_t(\vec{e}_t^{(l\pm 1)} \cdot \vec{\nabla}_t \ln n^2) r dr d\theta. \quad (72)$$

Here we have assumed $\vec{e}_t^{(l)}$ is normalized, i.e., $\langle \vec{e}_t^{(l)} | \vec{e}_t^{(l)} \rangle = 1$; the bra (\langle) and ket (\rangle) notation indicates a scalar product. Substitution of $\vec{e}_t^{(l\pm 1)} = \vec{e}_t^{(l)} + \delta\vec{e}_t^{(l\pm 1)}$ in Eq. 72 splits the integral into two integrals:

$$\delta\beta_{l\pm 1}^2 = \int_0^\infty \int_0^{2\pi} \vec{e}_t^{(l)*} \cdot \vec{\nabla}_t(\vec{e}_t^{(l)} \cdot \vec{\nabla}_t \ln n^2) r dr d\theta + \int_0^\infty \int_0^{2\pi} \vec{e}_t^{(l)*} \cdot \vec{\nabla}_t(\delta\vec{e}_t^{(l\pm 1)} \cdot \vec{\nabla}_t \ln n^2) r dr d\theta. \quad (73)$$

Substituting further $\vec{e}_t = F_l e^{il\theta} \vec{e}_\pm$ and $\delta\vec{e}_t^{(l\pm 1)} = G_{l\pm 2}(r) e^{i(l\pm 2)\theta} \vec{e}_\mp$ (Eq. 68), performing integration by parts, and noting that $F_l(r)$ and $G_{l\pm 2}(r)$ vanish at the end points of the integral, $r = 0$ and $r = \infty$, we arrive at Eq. 45:

$$\delta\beta_{l,\pm 1}^2 = -\pi \left[\int_0^\infty \frac{\partial \ln(n^2)}{\partial r} F_l(r) \left(\frac{dF_l(r)}{dr} \mp \frac{l}{r} F_l(r) \right) r dr + \int_0^\infty \frac{\partial \ln(n^2)}{\partial r} G_{l\pm 2}(r) \left(\frac{dF_l(r)}{dr} \mp \frac{l}{r} F_l(r) \right) r dr \right]; \quad (74)$$

we have assumed, as before, $n^2 = n^2(r)$ and also used the fact that $\vec{e}_\pm = 1/\sqrt{2}(\hat{x} \pm i\hat{y}) = 1/\sqrt{2}(\hat{r} \pm i\hat{\theta})e^{\pm i\theta}$ (in polar coordinates).

References

1. R. Bhandari, "Orbital Angular Momentum (OAM) Mode Mixing in a Bent Step Index Fiber in Perturbation Theory," in *IEEE Photonics Journal*, vol. 11, no. 3, pp. 1-21, June 2019, Art no. 7203421, doi: 10.1109/JPHOT.2019.2920097.
2. Allan W. Snyder and John D. Love, *Optical Waveguide Theory* Chapman and Hall, (1983).
3. G. Guerra, M.Lonardi, A. Galtarossa, L.A. Rusch, A. Bononi, and L. Palmieri, "Analysis of modal coupling due to birefringence and ellipticity in strongly guiding ring-core OAM fibers," *Opt. Express* **27**, 8308-8326 (2019).
4. S. Ramachandran and P. Kristensen. "Optical Vortices in Fiber", *Nanophotonics* **2**, 455-474 (2013).
5. H.Huang, G. Milione, M.P.J. Lavery, G. Xie, Y. Gongxiong Ren, Y. Cao, N. Ahmed, T. A. Nguyen, D. A. Nolan, M. Li, M. Tur, R. R. Alfano, and A. E. Willner, "Mode division multiplexing using an orbital angular momentum sorter and MIMO-DSP over a graded-index fibre", *Sci. Rep.*, vol. 5, art. no. 14931 (2015).
6. C. Brunet, B. Ung, P. Bélanger, Y. Messaddeq, S. LaRochelle and L. A. Rusch, "Vector Mode Analysis of Ring-Core Fibers: Design Tools for Spatial Division Multiplexing," in *Journal of Lightwave Technology*, vol. 32, no. 23, pp. 4648-4659, 1 Dec.1, 2014, doi: 10.1109/JLT.2014.2361432.
7. Y. Yue, Y. Yan, N. Ahmed, J. Yang, L. Zhang, Y. Ren, H. Hung, K.M. Birnbaum, B.I. Erkmen, S. Dolinar, M. Tur, and A.E. Willner, "Mode Properties and Propagation Effects of Optical Orbital Angular Momentum (OAM) Modes in a Ring Fiber," in *IEEE Photonics Journal*, vol. 4, no. 2, pp. 535-543, April 2012, doi: 10.1109/JPHOT.2012.2192474.
8. A.V. Volyar, V. Z. Zhilaitis, and V. G. Shvedov, "Optical Eddies in Small-Mode Fibers: II. The Spin-Orbit Interaction", *Optics and Spectroscopy* **86**, 593-598 (1999).
9. C.N. Alexeyev, M.S. Soskin, and A.V. Volyar, "Spin-orbit interaction in a generic vortex field transmitted through an elliptic fiber", *Semiconductor Phys. Quantum Electron. Optoelectron.***3**, 501-513 (2000).
10. R. Bhandari, "Spin Orbit and Contact interactions in Orbital Angular Momentum Modes in a Fiber", *Proc. of OSA-Frontiers in Optics/Laser Science*, September 2019, Paper JW4A.122.
11. , "Spin Orbit Interaction as a Perturbation in OAM Modes in an Optical Fiber" (under preparation).
12. P. Gregg, P. Kristensen, A. Rubano, S. Golowich, L. Marurucci, and S. Ramachandran, "Enhanced Spin Orbit Interaction of Light in Highly Confining Optical Fibers for Mode Division Multiplexing", *Nature Comm.*, Oct 2019; <https://doi.org/10.1038/s41467-019-12401-4>.
13. L.D. Landau and E.M. Lifshitz, *Quantum Mechanics* (Pergamon Press), 1977.
14. R. Bhandari, "Polarization-Induced Orbital Angular Momentum Field in a Multilayered Fiber", *Proc. of OSA-Frontiers in Optics*, September 2020, Paper JW6B.9.
15. A. Yariv and P. Yeh, *Photonics*, 6th Edition (Oxford University Press), 2007.
16. J. A. Buck, *Fundamentals of Fiber Fibers* (Wiley) 2004.